

Identifying Glyceraldehyde 3-Phosphate Dehydrogenase as a Cyclic Adenosine Diphosphoribose Binding Protein by Photoaffinity Protein–Ligand Labeling Approach

Kehui Zhang,^{†,‡} Wei Sun,^{‡,§} Lihong Huang,[‡] Kaiyuan Zhu,[‡] Fen Pei,[†] Longchao Zhu,[‡] Qian Wang,[‡] Yingying Lu,[‡] Hongmin Zhang,[§] Hongwei Jin,[†] Li-He Zhang,^{*,†} Liangren Zhang,^{*,†} and Jianbo Yue^{*,‡,Ⓛ}

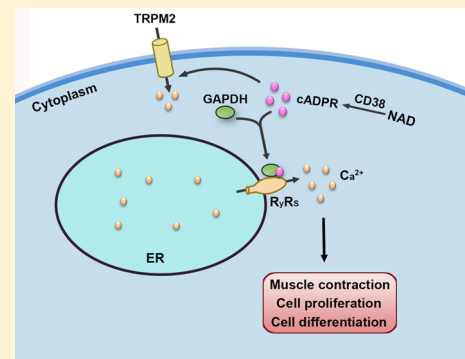
[†]State Key Laboratory of Natural and Biomimetic Drugs, School of Pharmaceutical Sciences, Peking University, Beijing 100191, China

[‡]Department of Biomedical Sciences, City University of Hong Kong, Hong Kong, China

[§]Department of Biology and Shenzhen Key Laboratory of Cell Microenvironment, South University of Science and Technology of China, Shenzhen 518052, China

Supporting Information

ABSTRACT: Cyclic adenosine diphosphoribose (cADPR), an endogenous nucleotide derived from nicotinamide adenine dinucleotide (NAD⁺), mobilizes Ca²⁺ release from endoplasmic reticulum (ER) via ryanodine receptors (RyRs), yet the bridging protein(s) between cADPR and RyRs remain(s) unknown. Here we synthesized a novel photoaffinity labeling (PAL) cADPR agonist, PAL-cIDPRE, and subsequently applied it to purify its binding proteins in human Jurkat T cells. We identified glyceraldehyde 3-phosphate dehydrogenase (GAPDH) as one of the cADPR binding protein(s), characterized the binding affinity between cADPR and GAPDH *in vitro* by surface plasmon resonance (SPR) assay, and mapped cADPR's binding sites in GAPDH. We further demonstrated that cADPR induces the transient interaction between GAPDH and RyRs *in vivo* and that GAPDH knockdown abolished cADPR-induced Ca²⁺ release. However, GAPDH did not catalyze cADPR into any other known or novel compound(s). In summary, our data clearly indicate that GAPDH is the long-sought-after cADPR binding protein and is required for cADPR-mediated Ca²⁺ mobilization from ER via RyRs.



INTRODUCTION

The cyclic adenosine diphosphoribose (cADPR)-mediated Ca²⁺ signaling pathway is involved in a wide variety of cellular processes,¹ e.g., abscisic acid signaling,² calorie restriction in gut stem cell,³ circadian clock in plants,⁴ and long-term synaptic depression in hippocampus.⁵ Many extracellular stimuli have been shown to induce cADPR production that leads to calcium release or influx, establishing cADPR as a second messenger.^{1b,6} CD38 is the dominant enzyme for synthesizing cADPR in mammalian systems, and CD38 knockout mice show a number of physiological defects, including metabolic disorder, impaired immune responses, and social behavioral changes.^{1a,7} Although the physiological importance of cADPR has been well-documented,^{3,4,8} the molecular mechanism mediating the cADPR signaling remains elusive.⁹

It has been shown that cADPR targets ryanodine receptors (RyRs) on the endoplasmic reticulum (ER) in many cell types,¹⁰ yet cADPR does not directly act on the receptor.¹¹ It is possible that cADPR binds to an accessory protein in the channel complex. Some candidates have been suggested, including calmodulin (CALM) and FK506-binding protein 12 (FKBP12).¹² Thus, far, this elusive cADPR binding protein

remains to be identified, let alone other regulators involved in cADPR signaling.

Here, we synthesized a photoaffinity labeling (PAL) cADPR analogue, PAL-cIDPRE, applied it to purify its novel binding proteins in human Jurkat T cells, and identified GAPDH as one of the cADPR-binding proteins.

EXPERIMENTAL SECTION

Chemistry. Compounds **9** and **11** were synthesized as described previously.¹³ Briefly, sodium benzoate (17.6 g, 122 mmol, 1.2 equiv) was added to a solution of epichlorohydrin (9.25 g, 100 mmol) in toluene (90 mL) along with tetra-*n*-butylammonium bromide as a catalyst. The mixture was stirred at 110 °C for 2 h followed by column chromatography (PE/EA) to purify compound **2**. Then, compound **2** (2.025 g, 9.15 mmol) in diemthylloxymethane (4 mL) was mixed with P₂O₅ (1.0 g) in chloroform (4 mL) in an ice-water bath for 2 h, followed by column chromatography (PE/EA) to purify compound **3**. Compound **3** (6.721 g, 30.38 mmol) and acetic anhydride (11 mL) were incubated with boron trifluoride–diethyl etherate complex (3 mL) at 0 °C for 2 h to generate compound **4**, which was then incubated with TMSBr in DCM to produce

Received: August 3, 2016

Published: December 12, 2016

compound 5. NHS ester of compound 9 (compound 10) was synthesized by adding NHS (1.2 equiv) and EDCl·HCl (1.2 equiv) and stirring in an ice-water bath for 16 h. Compound 12 was synthesized under conditions similar to those described previously,¹³ the deprotection of which produced compound 13. Compound 14 was synthesized by bis-phosphorylation of compound 13. The intramolecular cyclization of compound 14 produced N₃-cIDPRE (compound 15). ¹H NMR (400 MHz, MeOD) δ 8.58 (d, *J* = 23.6 Hz, 1H), 8.16 (d, *J* = 2.3 Hz, 1H), 6.23 (s, 1H), 6.15 (dd, *J* = 10.8, 5.7 Hz, 1H), 5.85 (dd, *J* = 22.3, 6.1 Hz, 1H), 5.39–5.33 (m, 1H), 5.23 (dd, *J* = 45.4, 10.9 Hz, 1H), 4.35 (t, *J* = 6.4 Hz, 1H), 3.87–3.74 (m, 3H), 3.58–3.31 (m, 4H), 1.53 (s, 3H), 1.37 (s, 3H). ³¹P NMR (162 MHz, decoupled with 1H, MeOD) δ –10.44 (d), –11.30 (d). HRMS (ESI-TOF[–]) calcd for C₁₇H₂₂N₇O₁₂P₂[–][(M – H)[–]]: 578.08072; found, 578.08088. NH₂-cIDPRE (compound 16) was synthesized through reduction of compound 15 via Staudinger reaction. PAL-cIDPRE (compound 17) was finally produced by incubating compound 10 with NH₂-cIDPRE. ³¹P NMR (162 MHz, decoupled with 1H, MeOD) δ –10.39 (d), –11.61 (d). HRMS (ESI-TOF[–]) calcd for C₂₆H₃₄N₇O₁₃P₂[–][(M – H)[–]]: 714.1695; found, 714.1704.

Cell Culture. Jurkat cells (from ATCC) were maintained in RPMI 1640 medium (RPMI 1640, powder, Invitrogen) with 10% fetal bovine serum (FBS, Invitrogen) and 1% penicillin–streptomycin (P/S, Invitrogen). HEK293 cells (from ATCC) were maintained in Dulbecco's modified Eagle medium (DMEM, powder, Invitrogen) with 10% fetal bovine serum (FBS, Invitrogen) and 1% P/S (Invitrogen). Human coronary artery smooth muscle cells (HCASMC), kindly provided by Dr. Guirong Li of the University of Hong Kong, were maintained in α -medium/F-12 medium (1:1) with 20% fetal bovine serum (FBS, Invitrogen), epidermal growth factor (EGF, recombinant human, 0.5 ng/mL), and fibroblast growth factor (FGF, recombinant human, 2 ng/mL). All cells were maintained at 37 °C with 5% CO₂ and 95% humidity and were passaged every 2 or 3 days.

Photoaffinity Purification. cIDPRE was used as a competitor of photoaffinity labeling probe PAL-cIDPRE. Briefly, for the control experiment, cIDPRE was incubated with cell lysate in a final concentration of 1 mM at 4 °C for 2 h, while for the experimental group, the same volume of MQ water was added instead of cIDPRE. Then, PAL-cIDPRE was added to the cell lysate in a final concentration of 10 μ M and incubated at 4 °C for 2 h. The samples were subsequently exposed to UV 365 nm at 4 °C for 30 min. Azide biotin was then added at a final concentration of 20 μ M, followed by the addition of catalyst. The catalyst composed of CuSO₄ (20 μ M) and TECP (tris(2-carboxyethyl)phosphine hydrochloride) (25 μ M) was applied to reduce Cu(II) to Cu(I), and THPTA (tris(3-hydroxypropyltriazolylmethyl)amine) (60 μ M) was added to stabilize Cu(I). After reacting at room temperature for 18 h, cold acetone was added to the reaction to precipitate proteins. Then, the pellet was washed with cold acetone three times and dissolved in 1% (w/v) SDS in PBS. The PAL-cIDPRE-bound proteins purified by streptavidin beads (Invitrogen) were eluted by boiling for 10 min in sample loading buffer and subjected to electrophoresis on 4–20% SDS polyacrylamide gradient gels. The gel was then visualized using silver staining or SYPRO Ruby staining. The protein bands which disappeared or became less abundant in the samples which were preincubated with cIDPRE were excised, in-gel digested with trypsin, and analyzed by LC-MS/MS on a ProteomeX-LTQ mass spectrometer (Institute of Biophysics, CAS, Beijing, China) to identify the interacting proteins. Database searches were performed by using MASCOT.

Western Blot Analyses. Cells were lysed in ice-cold lysis buffer (50 mM HEPES at pH 7.5, 0.15 M NaCl, 1 mM EDTA, 1% Nonidet P-40, 150 μ M PMSF, 10 mM NaF, 10 ng/mL leupeptin, 1 mM DTT, and 1 mM sodium vanadate) and passed through a 21 gauge needle several times to disperse any large aggregates. Protein concentrations of the cell lysates were determined by Bradford protein assay; 30 μ g of protein per lane was diluted in the standard SDS sample buffer and subjected to electrophoresis on 10% SDS

polyacrylamide gels or gradient gels (4–20%, purchased from Biorad). Proteins were then transferred to an Immobilon PVDF membrane (Millipore, Billerica, MA), blocked with 5% milk in TBST (20 mM Tris, 150 mM NaCl, pH 7.6), and incubated with the primary antibodies overnight. After washed with TBST, the blots were probed with a secondary antibody (1:5000 dilution) for detection by chemiluminescence. The antibodies used in the Western blot analyses were anti-GAPDH (1:1000 dilution), Sigma-Aldrich; anti-RyRs (1:500); and anti-VCP (1:1000), Santa Cruz Biotechnology, Inc.

Calcium Measurement. Calcium measurement was performed as described previously.¹⁴ Jurkat cells (2 \times 10⁵ cells/well) or HEK293 cells (6 \times 10⁴ cells/well) were plated in 24-well plates coated with 100 or 10 μ g/mL poly-L-lysine (purchased from Sigma), respectively. Human coronary artery smooth muscle cells were plated in 24-well plates without coating poly-L-lysine. Jurkat cells were incubated in serum-free medium overnight for adherence while HEK293 and HCASMCs were incubated in regular medium. The adherent cells were incubated with 2 μ M Fluo-2 AM in Hanks' balanced salt solution (HBSS) for 30 min in the dark at 37 °C. The cells were then washed with HBSS twice and incubated in 200 μ L of HBSS with or without calcium. Thereafter, the cells were put on the stage of an Olympus inverted epifluorescence microscope for measuring fluorescence intensity at 340 and 380 nm. Images were collected by a CCD camera and analyzed by the CellR software.

shRNA and Lentivirus Production and Infection. Three shRNA oligos against human GAPDH (Table S1) were cloned into the pLKO.1 vector for expressing shRNA. The lentivirus production and infection were performed as described previously.¹⁵ The shRNA knockdown efficiencies were assessed by Western blot analyses.

Immunocytochemistry. Immunocytochemistry was performed as described previously.¹⁶ Briefly, Jurkat cells (1 \times 10⁶ cells) were incubated with saponin (50 μ g/mL in PBS) at room temperature for 25 min, followed by cADPR, ADPR, or nicotinamide adenine dinucleotide (NAD⁺) (0.5 mM) treatment for indicated times. Cells were then fixed by paraformaldehyde (4% w/v) at room temperature for 30 min, spread on a gelatin-coated cover glass, and air-dried for 20 min. Thereafter, the cover glasses were blocked with 1% normal donkey serum, 1% BSA, and 0.1% Triton X-100 in PBS for 1 h, and incubated with primary antibodies (anti-GAPDH, G8795, Sigma-Aldrich, 1:200 dilution; anti-RyRs, sc-13942, Santa Cruz, 1:100 dilution) for 2 h, followed by incubation with secondary antibody (Alexa Fluor 488 goat anti-mouse IgG, A11008, 1:500 dilution; Alexa Fluor 555 donkey anti-rabbit IgG, A31572, Life Technologies, 1:500 dilution) incubation for 1 h. DAPI was used to stain the nuclei. Cells were imaged using a Zeiss LSM 880 Laser Scanning Microscope.

Super-Resolution Imaging. Super-resolution imaging was performed as described previously.¹⁷ Briefly, Jurkat cells were treated and immobilized on gelatin-coated cover glass as described in immunocytochemistry. After incubation with primary antibodies, the coverslips were incubated with secondary antibodies (Alexa Fluor 647 anti-rabbit for RYR primary antibody and Alexa Fluor 750 anti-mouse for GAPDH primary antibody) at room temperature for 2 h. Cells were then fixed with 3% PFA–0.05% glutaraldehyde at room temperature for 20 min and immersed in Stochastic optical reconstruction microscopy (STORM) imaging buffer (50 mM TCEP (phosphine tris(2-carboxyethyl)phosphine), 2 mM COT (cyclooctatetraene), 5 U/ml pyranose oxidase, 10% (w/v) glucose, 57 μ g/mL catalase, 1 mM ascorbic acid, and 1 mM methyl viologen in 200 mM Tris-HCl, pH 9.0). STORM images were acquired by the STORM system (NanoBioImaging Ltd., Hong Kong, China) with the dual-channel imaging of Alexa Fluor 647 and Alexa Fluor 750 immunolabeled samples. Prior to STORM imaging, the desired position was located using conventional fluorescence image with relatively low laser excitation power, typically 60 W/cm² for 656.5 nm laser in Alexa 647 channel and 80 W/cm² for 750 nm laser in Alexa 750 nm channel. During the STORM acquisition, the laser power was raised to 4 kW/cm² and 4.5 kW/cm², respectively. Each super-resolution image was reconstructed from a movie containing 20 000–30 000 frames recorded. The data was used to calculate a

two-dimensional (2D) Gaussian distribution that was assumed to center on the location of a single dye molecule. The final resolution was determined to be ~ 20 nm in both channels based on average fitting error.

Immunoprecipitation. Immunoprecipitation was performed as described previously.¹⁸ Briefly, anti-FLAG antibody beads (Invitrogen) and Protein A beads (GE Healthcare) were used to pull down FLAG-GAPDH and ryanodine receptors, respectively. FLAG-GAPDH overexpressing Jurkat cells were lysed, and 50 μ L of anti-FLAG beads were added to the lysate. The mixture was incubated with gentle rocking at 4 °C for 2 h and centrifuged for 30 s at 4 °C to discard the supernatant. The pellet was washed three times with PBST (PBS with 0.1% Tween 20), and 5 \times SDS sample buffer was added to the beads. The sample was heated in boiling water bath for 10 min, loaded on SDS-PAGE gel and subjected to Western blot analysis. Similarly, anti-RyRs primary antibody was incubated with Protein A beads with gentle rocking at 4 °C for 2 h. The beads were then washed and added to the lysate of Jurkat cells. The mixture was incubated at 4 °C for another 2 h, followed by cADPR (0.5 mM) treatment for the indicated times. Thereafter, the sample was immediately washed and heated with 5 \times SDS sample buffer in boiling water bath, loaded on SDS-PAGE gel, and subjected to Western blot analysis.

GAPDH Enzymatic Activity Assay. GAPDH enzymatic activity assay was performed as described previously.²¹ Briefly, 0.1 mL of NAD⁺ (7.5 mM in water), 0.03 mL of DTT (0.1 M in water), and 0.03 mL of GAPDH (0.083 mg/mL in PBS) were mixed with 0.87 mL of the sodium pyrophosphate buffer (0.015 M, pH 8.5, containing 0.03 M sodium arsenate). The mixture was then transferred to a cuvette and incubated in spectrophotometer at 25 °C for 3–5 min to determine a blank absorbance at 340 nm (A_{340}) in the absence of glyceraldehyde-3-phosphate (G3P). Afterward (time zero), 0.03 mL of 0.015 M G3P was added to the reaction, and A_{340} at 1 min intervals were recorded for 4 or 5 min. $\Delta A_{340}/\text{min}$ of the initial linear portion of the curve was determined. The extinction coefficient of NADH at 340 nm is 6.22 absorbance units/mmol when the path length is 10 mm, and 1 unit of enzymatic activity is defined as reduction of 1 μ M NAD⁺/min. Thus, the GAPDH enzymatic activity was calculated via the following equation:

$$\text{Units/mg} = \frac{\Delta A_{340}/\text{min}}{6.22 \times \text{mg GAPDH/mL reaction mixture}}$$

To evaluate the effects of cADPR on the enzymatic activity of GAPDH, cADPR at varied concentrations was added into the aforementioned reaction mixture before the start of the recording A_{340} .

HPLC Analysis of cADPR or NAD⁺ in GAPDH Enzymatic Reaction. HPLC analysis of cADPR or NAD⁺ in GAPDH enzymatic reaction was performed as described previously.²² Briefly, a column of AG MP-1 resin (10 \times 120 mm) was used to analyze cADPR, NAD⁺, or other adenine nucleotides. The elution was performed using a gradient of water/trifluoroacetic acid (TFA, 0.15 M in water) at a flow rate of 1 mL/min. The gradient was 0–10 min 0–15% TFA and 10–15 min 15–100% TFA. The UV detector of HPLC was set at 260 nm. Samples of GAPDH enzymatic reaction with or without cADPR were diluted with TFA and injected into HPLC for analysis.

Molecular Cloning. GAPDH cDNA was amplified from HeLa cell cDNA pools and subcloned into pRHSUL2 to engineer a His₆-tagged and a Sumo tag at the N-terminus of GAPDH or into pENTR-His₆-FLAG-C1 (Table S1). The His₆-FLAG-GAPDH sequence was then recombined into the pLenti-CMV-puro-DEST vector using the LR reaction, according to the manufacturer's instructions. The different segments of RyR2 were amplified from pCDNA-RyR2, a gift from Dr. King-Ho Cheung of University of Hong Kong, and subcloned into PGEX-4T1 to engineer a GST-tag at the N-terminus of RyR segments.

Mutagenesis. GAPDH^{His179Ala} and GAPDH^{Arg234Ala} were made by site-directed mutagenesis (Stratagene) as described previously.¹⁸ The primers used are listed in Table S1.

Recombinant Protein Purification. The His₆-Sumo-GAPDH construct was transformed into BL21 (DE3) *Escherichia coli* cells. Protein expression was induced by isopropyl-D-thiogalactopyranoside (IPTG) overnight. The *E. coli* cells were then lysed and sonicated in an ice-chilled container. The resulting cellular debris was removed by centrifugation at 17 000 rpm for 30 min, and the supernatant was loaded into a 5 mL HisTrap HP column (GE Healthcare). After extensive washing, His₆-Sumo-GAPDH protein was eluted and dialyzed overnight with SUMO protease buffer (20 mM Tris, pH 7.5, 0.1 M NaCl, SUMO protease) to cleave the His₆-Sumo tag from GAPDH. The reaction mixtures were again loaded to a HisTrap HP column, and the flowthrough was collected to obtain GAPDH protein. The GAPDH in the flow through was further purified by a HiTrap Q column (GE Healthcare), and concentrated by a 10 KD concentrator to about 20 μ g/mL.

Similarly, the GST-tagged RyR segments were expressed and purified by a 5 mL GSTrap column (GE Healthcare). The purified proteins were dialyzed and concentrated by a 10 KD concentrator to about 5–10 μ g/mL. All purified proteins were quantified by SDS-PAGE gel by using BSA as the standard.

Surface Plasmon Resonance (SPR) Assay. Interactions between GAPDH or its mutants and compounds were analyzed using the Biacore T200 system (GE Healthcare, Uppsala, Sweden) at 25 °C. Briefly, recombinant human GAPDH or its mutant proteins were immobilized on a sensor chip (CM5) using an amine coupling kit (GE Healthcare, Buckinghamshire, UK). Final immobilized GAPDH levels were typically ~ 15 000 RU. Subsequently, compounds were injected as analytes at various concentrations and 20 mM Tris-HCl (pH 7.5 with 0.05% surfactant P20) was used as running buffer. For binding affinity studies, analytes were applied at indicated concentrations in running buffer at a flow rate of 30 μ L/min with a contact time of 60 s and a dissociation time of 60 s. Chip platforms were washed with running buffer.

Molecule Docking and Molecular Dynamic Simulations. The crystal structure of GAPDH was obtained from RCSB Protein Data Bank (<http://www.pdb.org>, PDB ID: 1U8F). The protein was prepared with the Protein Clean tools in Discovery Studio 2.5 (Accelrys, San Diego, USA). In the preparation step, the CHARMm force field was applied, the protein protonated, hydrogen atoms added, and all water molecules and the original ligand NAD⁺ removed by using the protein preparation protocols. The structure of cADPR was sketched in ChemBioDraw Ultra (<http://www.cambridgesoft.com>). Then, the preparation and 1000 steps of steepest descent followed by 1000 steps of conjugate gradient minimization were carried out for cADPR using Sybyl X 1.1.2 Molecular Modeling Suite.¹⁹ The molecular docking simulation was carried out with GOLD docking program.²⁰ GOLD is the abbreviation of genetic optimization for ligand docking, which is a genetic algorithm for docking flexible ligands into protein binding sites containing flexible side chains of the target protein. In the GOLD docking program, the initial position of NAD⁺ was used to define the center of the binding site, and the pocket was defined as all residues within a radius of 8.0 Å. Other parameters were remained as default. The docking results were indicated by GoldScore fitness calculated from contributions of hydrogen bonds and van der Waals interactions between GAPDH and cADPR.

The best binding mode obtained from molecule docking was chosen as initial structure for molecular dynamics simulation. Molecular dynamics (MD) simulation was performed with AMBER 11 molecular simulation package.²¹ To obtain molecular mechanical parameters for cADPR, *ab initio* quantum chemical methods were employed using Gaussian 09 program.²² The geometry was fully optimized, and the electrostatic potentials around them were then determined at the HF/6-31G* level of theory. The RESP strategy²³ was used to obtain the partial atomic charges.

The starting structure of cADPR–GAPDH complex obtained by docking was solvated in TIP3P water using a octahedral box, which

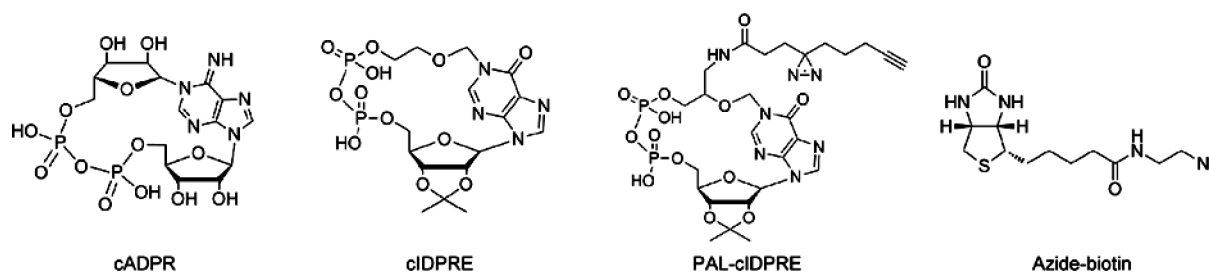


Figure 1. Structures of cADPR, cIDPRE, PAL-cIDPRE, and azide-biotin.

was extended 8 Å away from any solute atom. To neutralize the negative charges of simulated molecules, Na⁺ counterion was placed next to each phosphate group. MD simulation was carried out by using SANDER module of AMBER 11. The calculations began with 500 steps of steepest descent followed by 500 steps of conjugate gradient minimization with a large constraint of 500 kcal mol⁻¹ Å⁻² on the complexes atoms. Then, 1000 steps of steepest descent followed by 1500 steps of conjugate gradient minimization with no restraint on the complex atoms were performed. Subsequently, after 20 ps of MD, during which the temperature was slowly raised from 0 to 300 K with weak (10 kcal mol⁻¹ Å⁻²) restraint on the complex, the final unrestrained production simulations of 10.0 ns was carried out at constant pressure (1 atm) and temperature (300 K). In the entire simulation, SHAKE was applied to all hydrogen atoms. Periodic boundary conditions with minimum image conventions were applied to calculate the nonbonded interactions. A cutoff of 10 Å was used for the Lennard-Jones interactions. The final conformations of the complexes were produced from the 1000 steps of minimized averaged structure of the last 5.0 ns of MD.

GST *in Vitro* Pull down Assay. Binding between GAPDH and RyR segments was assessed by the GST fusion protein pulldown assay as described previously.²³ Briefly, GST-tagged RyR segment protein (10 μg) was incubated with 10 μL of Glutathione Sepharose 4 Fast Flow for 30 min on ice followed by extensive washing. Thereafter, BSA (25 μg) with or without GAPDH (10 μg) was added to the beads followed by extensive washing. The RyR segment protein and its associated proteins were then eluted by glutathione and analyzed by SDS-PAGE, coomassie brilliant blue staining (for RyR detection), and immunoblot (for GAPDH detection).

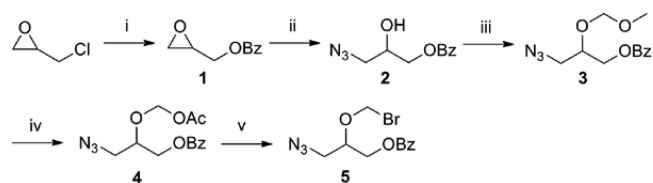
Native PAGE. A discontinuous native gel was applied to analyze the oligomerization of GAPDH. The recipe for a 5 mL native PAGE stacking gel comprised 0.375 M Tris-HCl (pH8.8), 4.275 mL; acrylamide/bis-acrylamide (30%/0.8%), 0.67 mL; 10% ammonium persulfate, 0.05 mL; and TEMED, 5 μL. For a 10 mL 8% separating gel, the recipe comprised 0.375 M Tris-HCl (pH8.8), 7.29 mL; acrylamide/bis-acrylamide (30%/0.8%), 2.6 mL; 10% ammonium persulfate, 0.1 mL; and TEMED, 10 μL. The 2× sample buffer was 0.625 M Tris-HCl (pH8.8) containing 50% glycerol and 1% Coomassie Brilliant Blue G-250. As previously reported,²⁴ the anode buffer for native gel was 100 mM Tris-HCl, pH 8.8. The cathode buffer was 100 mM histidine with 0.002% Coomassie Brilliant Blue G-250, pH 8.0 (adjusted by Tris base). After electrophoresis, the gel was either directly scanned or transferred to PVDF membrane for Western blot analysis.

RESULTS

Design and Synthesis of a Novel Photoaffinity Labeling cADPR Analogue, PAL-cIDPRE. Several cADPR analogues have been synthesized,²⁵ among which cIDPRE, a structural simplified analogue, is a membrane-permeable cADPR agonist in Jurkat T cells (Figure 1).²⁶ Based on the structure–activity relationship of these cADPR analogues, we found that the configuration of the N1-glycosyl moiety on the northern ribose of cADPR is not critical for its Ca²⁺ mobilization ability. Thus, we designed and synthesized a

photoaffinity labeling cADPR analogue based on cIDPRE and referred it as PAL-cIDPRE (Figure 1 and Schemes 1–3). PAL-

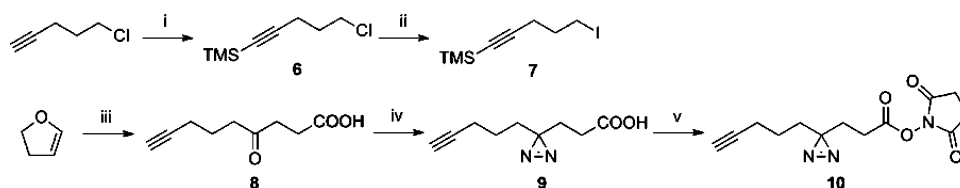
Scheme 1. Synthesis of Compound 5^a



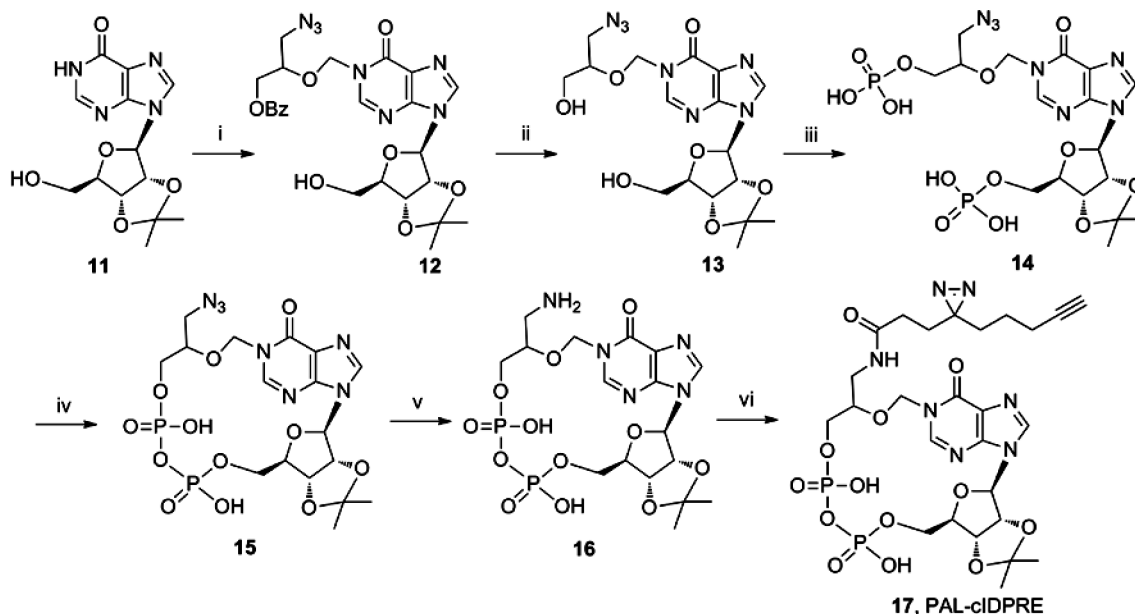
^aReagents and conditions: (i) PhCO₂Na, toluene, reflux; (ii) NaN₃, EtOH, reflux; (iii) P₂O₅, (CH₃O)₂CH₂, 0°C; (iv) Ac₂O, BF₃, 0°C; (v) TMSBr, CH₂Cl₂, reflux.

cIDPRE is composed of an amino-cIDPRE ligand moiety and a photoreactive group carrying a clickable terminal. Notably, the ligand moiety has the northern ribose replaced by a branched ether chains. Its photoreactive group, diazirine, could bind the related protein under UV irradiation, and its terminal alkyne group could connect with a biotin moiety by click reaction. Biotin was altered to carry a corresponding clickable terminal of an azide group and was separately synthesized (Figure S1A). The structure of PAL-cIDPRE was characterized by ¹H, ¹³C, ³¹P NMR, and high-resolution mass spectrometry (Figure S1B–F). In principle, after PAL-cIDPRE interacts with its receptor(s), applied UV irradiation could generate a reactive species that covalently binds the probe to its receptor, and the binding protein(s) could then be purified and identified.

Pharmacological Characterization of PAL-cIDPRE. We next examined the ability of PAL-cIDPRE to induce Ca²⁺ release in human Jurkat T cells. The PAL-cIDPRE markedly increased cytosolic Ca²⁺ in a concentration-dependent manner either in the presence or absence of extracellular Ca²⁺, and the cytosolic Ca²⁺ increase observed in the presence of extracellular Ca²⁺ was significantly higher and sustained compared to that in the absence of extracellular Ca²⁺ (Figure 2A), suggesting that Ca²⁺ influx also contributes. Pretreating cells with thapsigargin, a specific SERCA inhibitor, abolished PAL-cIDPRE-induced Ca²⁺ increase in the absence of extracellular Ca²⁺, consistent with the fact that cADPR triggers Ca²⁺ release from the ER pools (Figure 2B). These data also indicate that PAL-cIDPRE induces Ca²⁺ release from ER pools, accompanied by extracellular Ca²⁺ influx. Ample evidence indicates that cADPR targets ryanodine receptors (RyRs) on the ER membrane for Ca²⁺ mobilization in many cell types.²⁷ Indeed, pretreatment with a RyR antagonist, high concentrations of ryanodine, or a cADPR antagonist, 8-Br-cADPR (Figure 2C), or RyR2 and RyR3 double knockdown²⁸ (Figure 2D) significantly inhibited PAL-cIDPRE-induced Ca²⁺

Scheme 2. Synthesis of Compounds 7 and 10^{4a}

^{4a}Reagents and conditions: (i) *n*-BuLi, TMSCl, -78°C ; (ii) Na, acetone, reflux; (iii) a. *t*-BuLi, 7, -78°C ; b. Jones' reagent; (iv) a. NH_3 (liquid), $\text{NH}_2\text{OSO}_3\text{H}$; b. I_2 , Et_3N ; (v) NHS, EDCl, 0°C .

Scheme 3. Synthesis of a Novel Photoaffinity Labeling cADPR Analogue, PAL-cIDPRE^{4a}

^{4a}Reagents and conditions: (i) 5, DBU, -20°C ; (ii) NH_3/MeOH ; (iii) POCl_3 , DIPEA, 0°C ; (iv) EDCl, microwave; (v) Ph_3P , rt; (vi) 10, Et_3N .

increases in Jurkat cells. Collectively, it is clear that PAL-cIDPRE is a cell permeant cADPR agonist and can trigger Ca^{2+} releases via RyRs.

Identification of GAPDH as a cADPR-Binding Protein.

Subsequently, we incubated PAL-cIDPRE with Jurkat cell crude extracts in the presence or absence of cIDPRE, followed by UV irradiation to generate the reactive species that cross-links the cIDPRE to its target receptors. Cu(I) and azide-biotin were then added to the mixture to form a triazole ring between biotin and the protein-cIDPRE complexes via click reaction. Afterward, the cIDPRE-bound proteins were purified by streptavidin-coupled Dynabeads and analyzed by mass spectrometry analyses (Figure 3A). As shown in Figures 3B (right panel) and S2A,B, several protein bands appeared in samples treated with PAL-cIDPRE alone, and two of these bands were significantly competed off by cIDPRE preincubation, suggesting that these two PAL-cIDPRE labeled proteins are specific. Surprisingly, one of the proteins (lane 1 in Figures 3B and S2A) turned out to be glyceraldehyde 3-phosphate dehydrogenase (GAPDH) by mass spectrometry analyses (Figure S2C,D), and Western blot analyses confirmed that GAPDH in Jurkat cell crude extract was specifically labeled with PAL-cIDPRE, which was competed off by cIDPRE preincubation (left panel in Figure 3B). We then characterized the affinity between wildtype GAPDH protein and cADPR by a surface plasmon resonance (SPR) assay and found that cADPR specifically bound to the

recombinant GAPDH proteins (Figure S3) immobilized on the CMS chip. The calculated K_D value of cADPR from the SPR assay was around $8.59\ \mu\text{M}$ (Figure 3C). As a control, ADPR, a nucleotide derived from NAD^+ or cADPR, showed no specific binding to GAPDH immobilized on the CMS chip by SPR assay (Figure S4). These data suggest that GAPDH is a specific cADPR-binding protein.

Mapping cADPR's Binding Residues in GAPDH. We also performed the molecule docking and molecular dynamic simulations to predict the binding sites in GAPDH for cADPR based on the crystal structures of GAPDH²⁹ and cADPR.³⁰ As shown in Figure 4A, cADPR binding to GAPDH could induce a conformational change of GAPDH, and potential salt-bridges exist between two H atoms of N2,N3 from guanidine group of Arg234 in GAPDH and the O4 from cADPR, and hydrogen bonds between the H atom of N1 from iminazole of His179 in GAPDH and the O5 from cADPR, with distances of 1.8, 2.0, and 1.9 Å, respectively (Figure 4A). This analysis suggests that Arg234 and His179 in GAPDH might be the potential binding sites for cADPR. We therefore purified recombinant GAPDH^{Arg234Ala} and GAPDH^{His179Ala} proteins (Figure S3), and both mutant proteins existed in the form of tetramers *in vitro*, suggesting that both are properly folded (Figure S5). As expected, the SPR assay showed that the K_D value of cADPR to GAPDH^{His179Ala} mutant protein was markedly increased to $82\ \mu\text{M}$ (Figure 4B), and cADPR even did not bind specifically

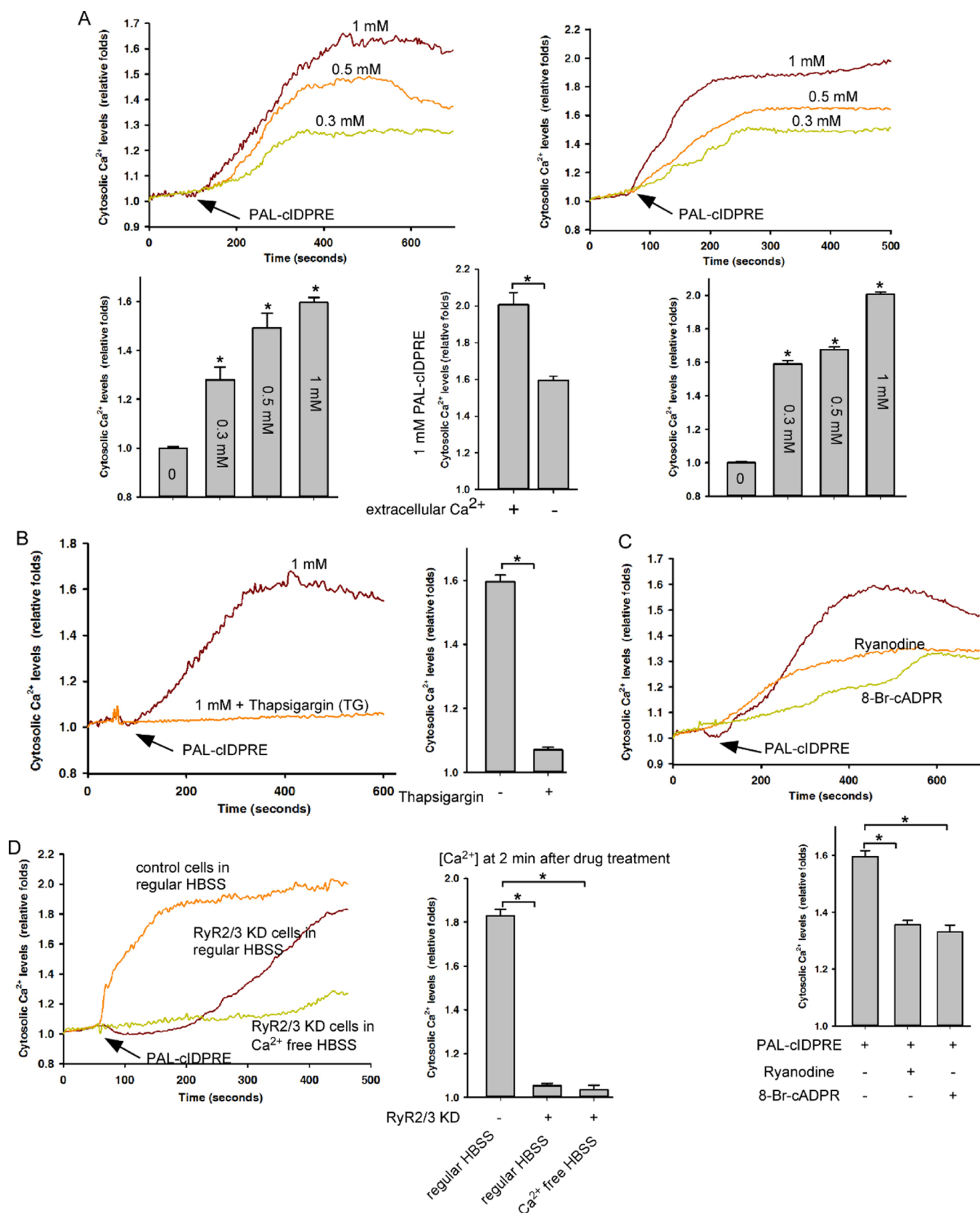


Figure 2. PAL-cIDPRE is a cell permeable cADPR agonist. (A) PAL-cIDPRE markedly induced cytosolic Ca²⁺ increases in human Jurkat T cells in the absence of (left panel) or presence of (right panel) extracellular Ca²⁺. (B) PAL-cIDPRE (1 mM) induced cytosolic Ca²⁺ increase in Jurkat cells was blocked by thapsigargin (1 μ M) pretreatment. (C) PAL-cIDPRE (1 mM) markedly induced cytosolic Ca²⁺ increase in human Jurkat T cells in the absence of extracellular Ca²⁺, which was significantly inhibited by ryanodine (10 μ M) or 8-Br-cADPR (200 μ M). (D) RyR2/RyR3 double knockdown in Jurkat cells markedly inhibited PAL-cIDPRE (1 mM) induced cytosolic Ca²⁺ increase. Quantification of intracellular Ca²⁺ peak values are expressed as mean \pm S.D., $n = 3$ (15–30 cells in each independent experiment). *, $P < 0.05$.

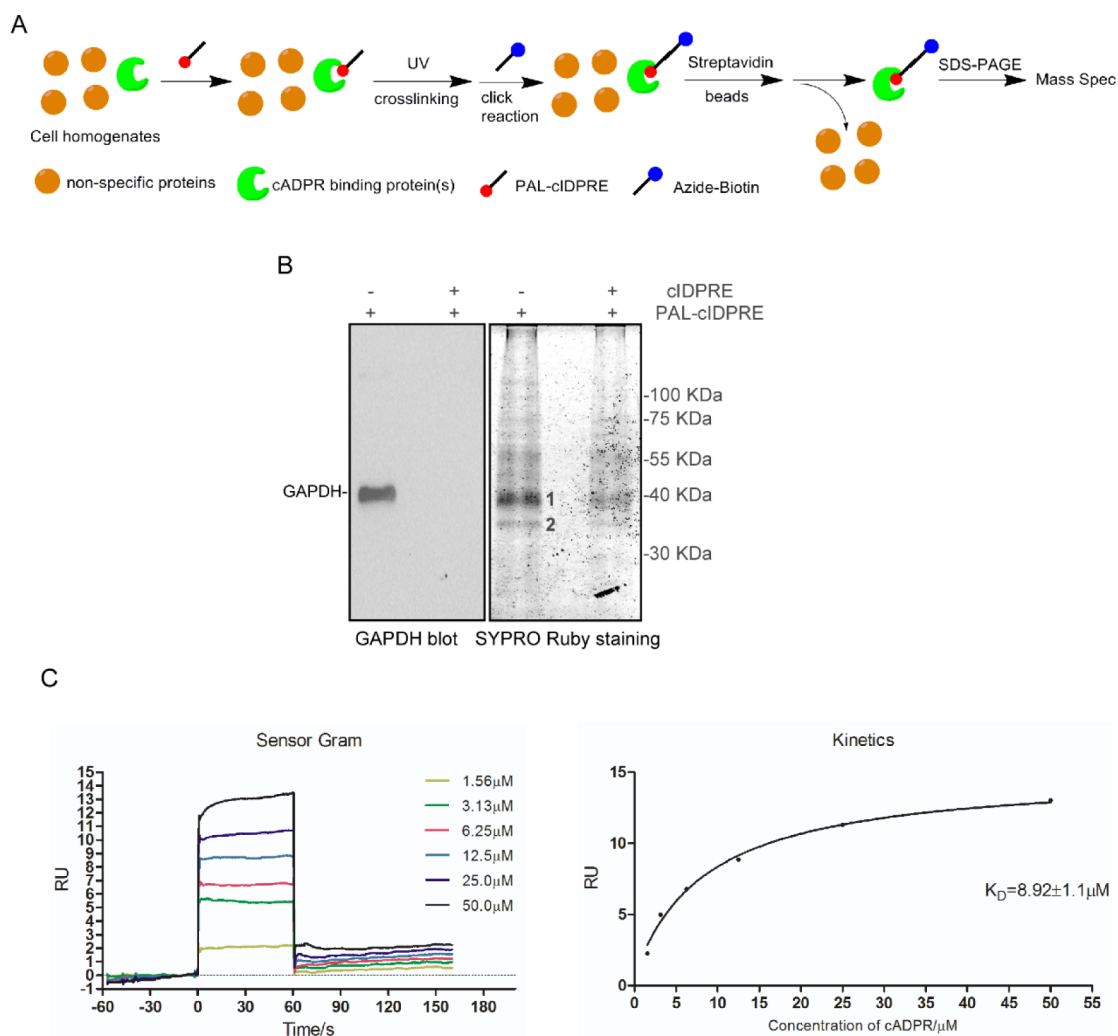


Figure 3. Identification of GAPDH as a novel cADPR-binding protein by a photoaffinity purification approach. (A) Schematic of identifying cADPR binding protein by a photoaffinity purification approach. (B) Identification of GAPDH as the binding protein of PAL-cIDPRE (20 μM) in Jurkat cell crude extract, which was competed off by cIDPRE (1 mM) preincubation. Left panel: GAPDH immunoblot analysis of the PAL-cIDPRE complex; right panel: SYPRO Ruby staining of the PAL-cIDPRE complex. (C) Characterization of the binding affinity between cADPR and GAPDH by a SPR assay; data are representative of three independent experiments.

to GAPDH^{Arg234Ala} mutant protein (Figure 4C). These data indicate that both His179 and Arg234 in GAPDH are indeed two key residues for the interaction between cADPR and GAPDH. We also used NAD⁺, a known binding partner of GAPDH, in the SPR assay as a control and found that His179Ala or Arg234Ala mutation did not significantly affect the binding affinity between NAD⁺ and GAPDH (Figure 5A–C). Thus, these data further indicate that His179 and Arg234 in GAPDH are specific for its binding with cADPR, not NAD⁺.

Effects of cADPR on GAPDH's Catalytic Activity.

GAPDH, a traditional “housekeeping gene”, plays essential role in glycolysis and gluconeogenesis. GAPDH catalyzes oxidative phosphorylation of D-glyceraldehyde 3-phosphate (G3P) to 1,3-bisphospho-D-glycerate with inorganic phosphate as the cosubstrate and NAD⁺ as coenzyme, in which NAD⁺ can receive a hydride ion to be reduced to NADH³¹ (Figure S6A). We, thus, performed a standard *in vitro* GAPDH assay, GAPDH + G3P \pm NAD⁺, in the presence or absence of cADPR and assessed GAPDH enzymatic activity by measuring rate of NAD⁺ conversion to NADH. We found that cADPR at

higher concentration only marginally inhibited GAPDH's oxidative phosphorylation activity (Figures 6A and S6B). In addition, we analyzed the aforementioned reactions by HPLC to detect the reaction end products. Interestingly, GAPDH + G3P + NAD⁺ reaction produced not only the NADH peak but also ADPR and nicotinamide peak (Figure S6C), indicating that GAPDH can hydrolyze NAD⁺ to nicotinamide and ADPR. Yet, in reaction of GAPDH + G3P + cADPR \pm NAD⁺, GAPDH failed to catalyze or hydrolyze cADPR into ADPR or any other compounds (Figure 6B). These data suggest that cADPR is not the catalytic substrate of GAPDH in glycolysis, at least *in vitro*.

GAPDH Is Required for cADPR-Mediated Ca²⁺ Release. GAPDH is actually more than just a catalyzing enzyme in glycolysis, functioning across the major cellular compartments to be involved in many important cellular events.³² We reason that cADPR might bind to GAPDH to trigger Ca²⁺ release from ER. As expected, GAPDH knockdown markedly inhibited NPE-cADPR- or PAL-cIDPRE-induced cytosolic Ca²⁺ increase in Jurkat cells (Figure 7A,B), RyR3-expressing HEK293 cells (Figure 7C), or human

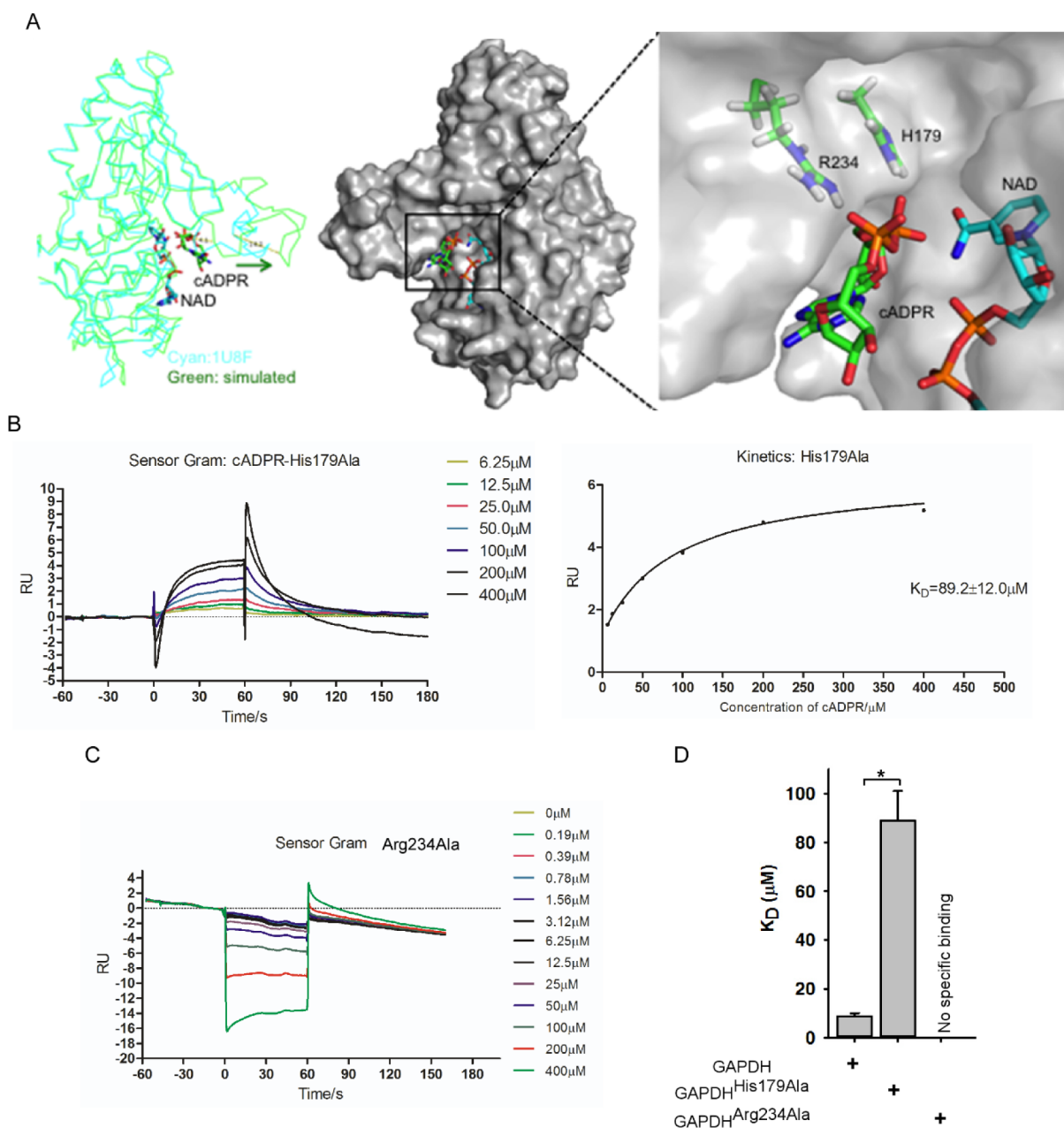


Figure 4. His179 and Arg234 in GAPDH are required for the binding between GAPDH and cADPR. (A) Simulated GAPDH in complex with cADPR (colored in green) was superimposed onto GAPDH (monomer) in complex with NAD (PDB ID: 1U8F, colored in cyan) in left panel. The conformational change upon the binding of cADPR is indicated by the green arrow. cADPR was shown as ball-and-stick models with green carbons. Residues His179 and Arg234 showed charge interactions with the phosphate backbone of cADPR (right panel). NAD was also shown for comparison. (B–D) The binding affinity between GAPDHHis179Ala (B) or GAPDHArg234Ala (C) and cADPR was significantly decreased compared to that of GAPDH wildtype protein (D). Quantification of K_D are expressed as mean \pm S.D., $n = 3$. *, $P < 0.05$.

coronary artery smooth muscle (HCVSM) cells (Figure 7D). In contrast, GAPDH knockdown did not affect ATP- or histamine-induced Ca^{2+} increases in Jurkat cells (Figure S7A,B), suggesting that GAPDH is not involved in inositol trisphosphate (IP_3)-mediated Ca^{2+} mobilization. Likewise, GAPDH knockdown did not change ionomycin or thapsigargin induced Ca^{2+} increases (Figure S7C,D), suggesting that the ER Ca^{2+} pool is not affected by GAPDH depletion. In addition, GAPDH knockdown had little effects on store-operated Ca^{2+} entry (SOCE) (Figure S7E). Notably, ATP level in GAPDH knockdown cells was much lower than that in control cells (Figure S7F), and these cells started to

die after 3 passages. Taken together, these data suggest that GAPDH is specifically involved in cADPR-mediated cytosolic Ca^{2+} mobilization.

cADPR Transiently Increases the Interaction between GAPDH and RyRs. Since cADPR incites Ca^{2+} release from ER via RyRs but does not directly bind to RyRs, we speculate that GAPDH might be the bridging protein between cADPR and RyRs. Not surprisingly, we found that there is a basal interaction between GAPDH and RyRs in Jurkat cells (Figure S8A), and cADPR treatment transiently but markedly increased the interaction between RyRs and GAPDH as shown by the Co-IP experiments (Figures 8A and S8B).

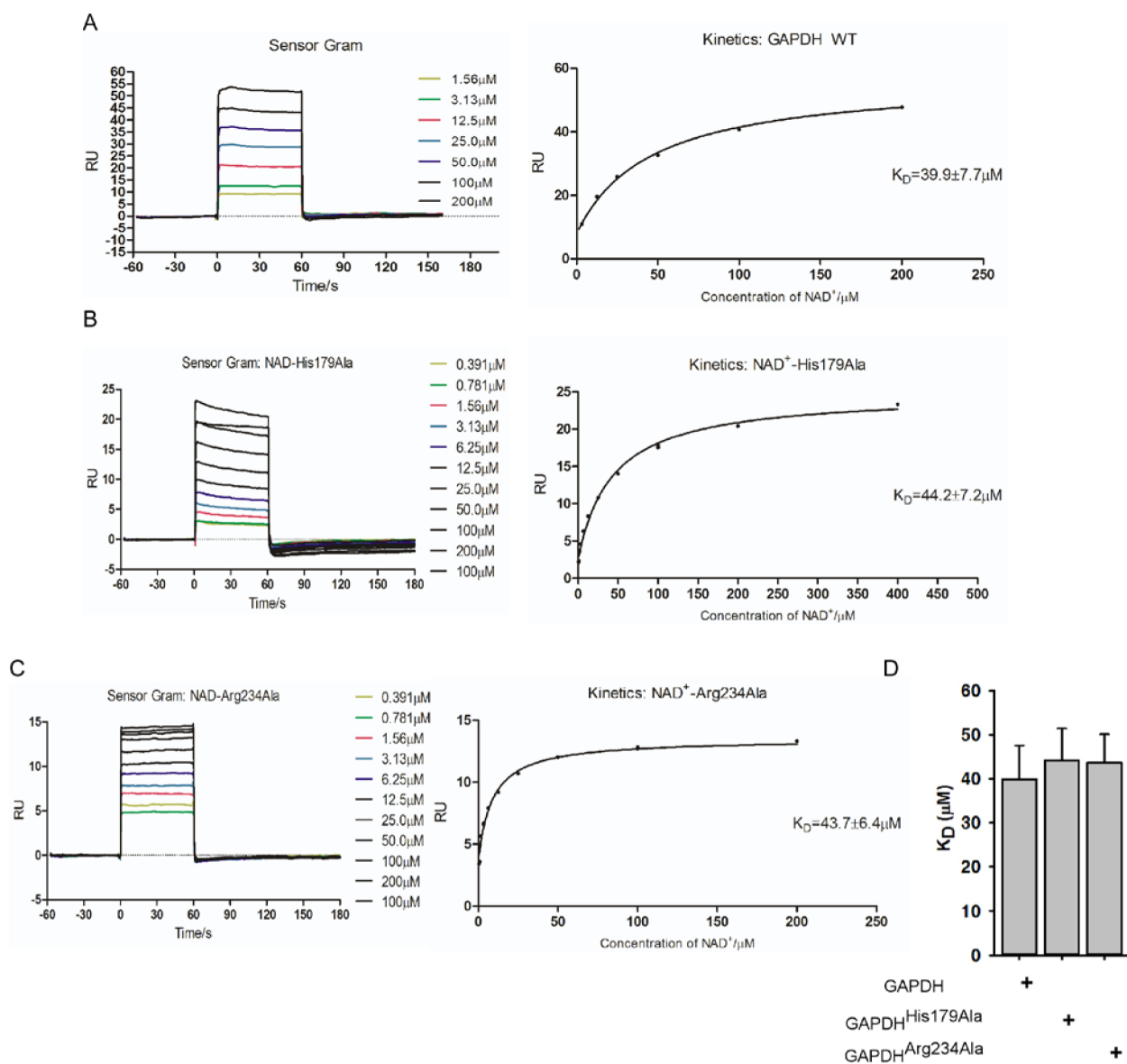


Figure 5. His179 and Arg234 in GAPDH are not required for the binding between GAPDH and NAD⁺. (A–C) Characterization of the binding affinity between NAD⁺ and GAPDH (A), GAPDH^{His179Ala} (B), or GAPDH^{Arg234Ala} (C) by a SPR assay. (D) Quantification of K_D are expressed as mean \pm S.D., $n = 3$.

Furthermore, we treated Jurkat cells with saponin to partially permeabilize cell membrane, which enables the cytosolic GAPDH to leak out of the cells but spares the organelle or membrane associated pools. Strikingly, we found that addition of cADPR to the permeabilized cells transiently induced the colocalization of GAPDH with RyRs by immunostaining analyses with antibodies against GAPDH and RyRs, respectively (Figure 8B and S8C). Preincubating the antibodies with respective peptides abolished the positive staining pattern in Jurkat cells (Figure S8D), supporting the specificity of both antibodies. Surprisingly, washing saponin-treated cells with PBS abolished cADPR-induced colocalization of GAPDH with RyRs (Figure S8E). These data suggest that cADPR forms complex with the leaked GAPDH extracellularly and that the cADPR–GAPDH complex then transiently flows back into cells to interact with RyRs. As controls, ADPR, a metabolite of cADPR or NAD⁺, or NAD⁺ itself, failed to induce the localization of GAPDH with RyRs in saponin-treated Jurkat cells (Figure S8F,G). Furthermore, super-

resolution imaging analyses confirmed that GAPDH was transiently colocalized with RyRs in saponin-treated Jurkat cells upon cADPR treatment (Figure 8C). Collectively, these data indicate that cADPR treatment transiently increases the interaction between GAPDH and RyRs *in vivo*.

Mapping the Regions in RyRs for GAPDH Interaction. To assess which region(s) in RyRs is(are) involved in the interaction with GAPDH, we purified several GST-fusion recombinant proteins covering different RyR2 regions located at its N-terminal cytosolic domain except regions from amino acid residues 2644–3511, which appeared to be in the inclusion body (Figure 9A). The *in vitro* GST pull-down experiments were subsequently performed to determine the region in RyRs where GAPDH binds. As shown in Figure 9A (right panel), regions 6 (residues 2210–2643) and 7 (residues 3512–4560), in RyR2 exhibited weak interaction with GAPDH. Moreover, addition of cADPR to the binding complex increased the binding affinity between region 7 (residues 3512–4560) but not that of region 6 (residues

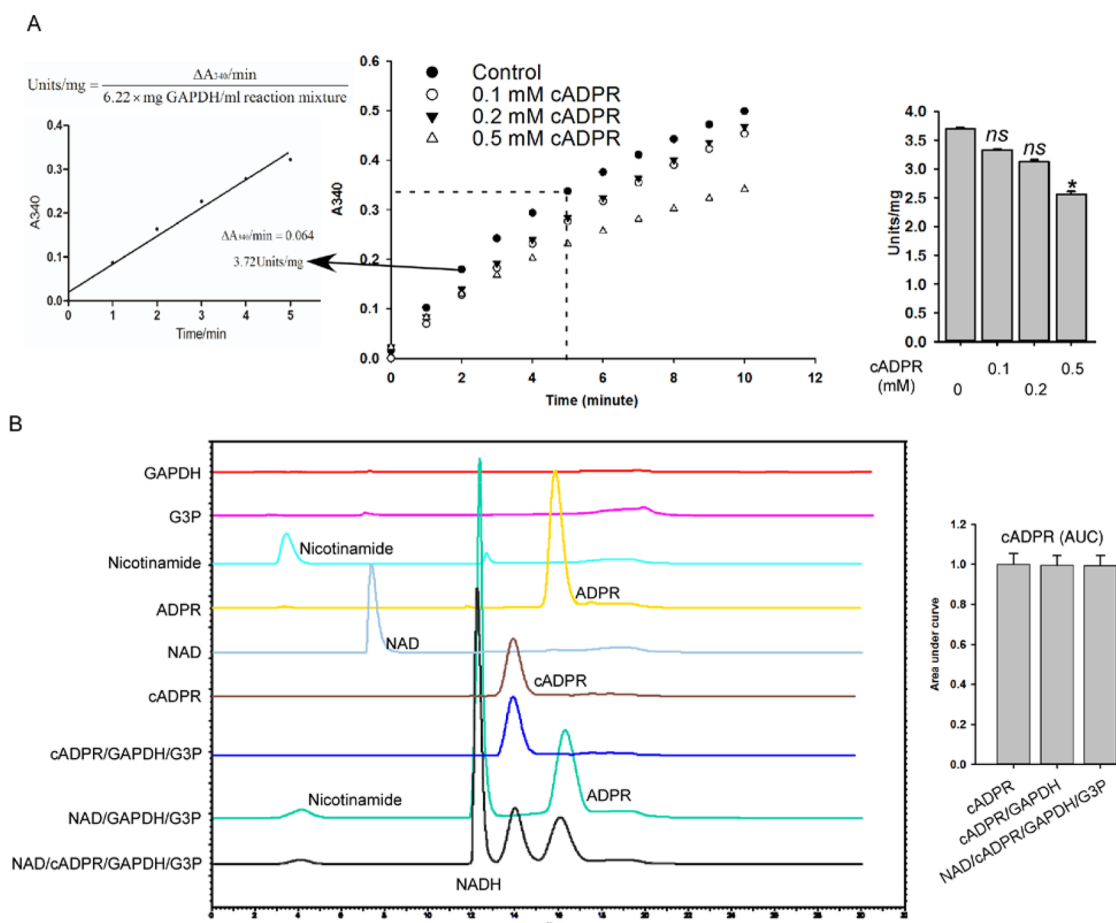


Figure 6. cADPR is not the catalytic substrate of GAPDH. (A) *In vitro* GAPDH assay (GAPDH + G3P ± NAD⁺) in the presence or absence of cADPR was performed, and GAPDH enzymatic activity was assessed by measuring rate of NAD⁺ conversion to NADH (A340). cADPR at higher concentration marginally inhibited GAPDH's oxidative phosphorylation activity. (B) HPLC analysis of the GAPDH + G3P ± NAD⁺ ± cADPR reaction. Quantification of the cADPR peak in the reactions are expressed as area under curve (AUC) ± S.D., *n* = 3.

2210–2643) and GAPDH (Figure 9B). Subsequently, we assessed which domain(s) in GAPDH is(are) involved in the interaction with the region 7 (residues 3512–4560) in RyR2. Surprisingly, the *in vitro* GST pull-down experiments showed that the catalytic domain, not NAD⁺ binding domain, of GAPDH bound with region 7 (residues 3512–4560) in RyR2 (Figure 9C). Notably, region 7 is actually the central domain of RyRs. Most recently, the structures of RyRs in both the open and closed states were determined by single-particle electron cryomicroscopy, and it has been shown that the rotation of central domain of RyRs leads to the dilation of the cytoplasmic gate through coupled motions.³³ Nevertheless, these data suggest that the interaction between GAPDH and RyRs is specific and that cADPR treatment increases the interaction between GAPDH and RyRs *in vitro*.

DISCUSSION

Here we identified GAPDH as one of cADPR's binding protein(s) by photoaffinity protein–ligand labeling approach (Figures 3 and S2) and demonstrated that GAPDH is required for cADPR-induced Ca²⁺ release from ER in several cell lines (Figure 7). Notably, GAPDH did not catalyze cADPR into any other known or novel compound(s) (Figure 6B). Moreover, we found that cADPR transiently increased the interaction between GAPDH and RyRs both *in vitro* and *in vivo* (Figures 8 and 9). Taken together, our data indicate

that cADPR targets GAPDH to RyRs and thus triggers Ca²⁺ release from ER.

Interestingly, another protein (band 2 in Figures 3B and S2A) might also be a specific PAL-cIDPRE's binding protein since it was competed off by cIDPRE preincubation, yet its identity remained to be determined due to its low abundance after the final purification step. Efforts will be continued to identify this protein in the near future. Upon its identification, its role in cADPR-mediated Ca²⁺ mobilization and its relationship with GAPDH and RyRs upon cADPR treatment will be studied accordingly.

It has been shown that cADPR specifically binds to microsomes from sea urchin eggs with *K_D* around 17 nM.³⁴ In human Jurkat cells, Guse et al. found that stimulation of the T-cell receptor markedly increased intracellular cADPR levels from 0.5 to 2 μM, which is responsible for subsequent Ca²⁺ signaling and T cell activation.³⁵ Here, we found that the binding affinity between cADPR and GAPDH is around *K_D* = 9 μM (Figure 4C). Obviously, the aforementioned mysterious protein(s) (band 2 in Figures 3B and S2A) might be involved in the interaction between cADPR and GAPDH as well. In addition, it is well-recognized that it is difficult not to change the biological functionality of molecules during the process of immobilizing the molecules to the sensor chip.³⁶ Thus, the binding affinity between cADPR and GAPDH might be underestimated in SPR assay compared to that *in vivo*.

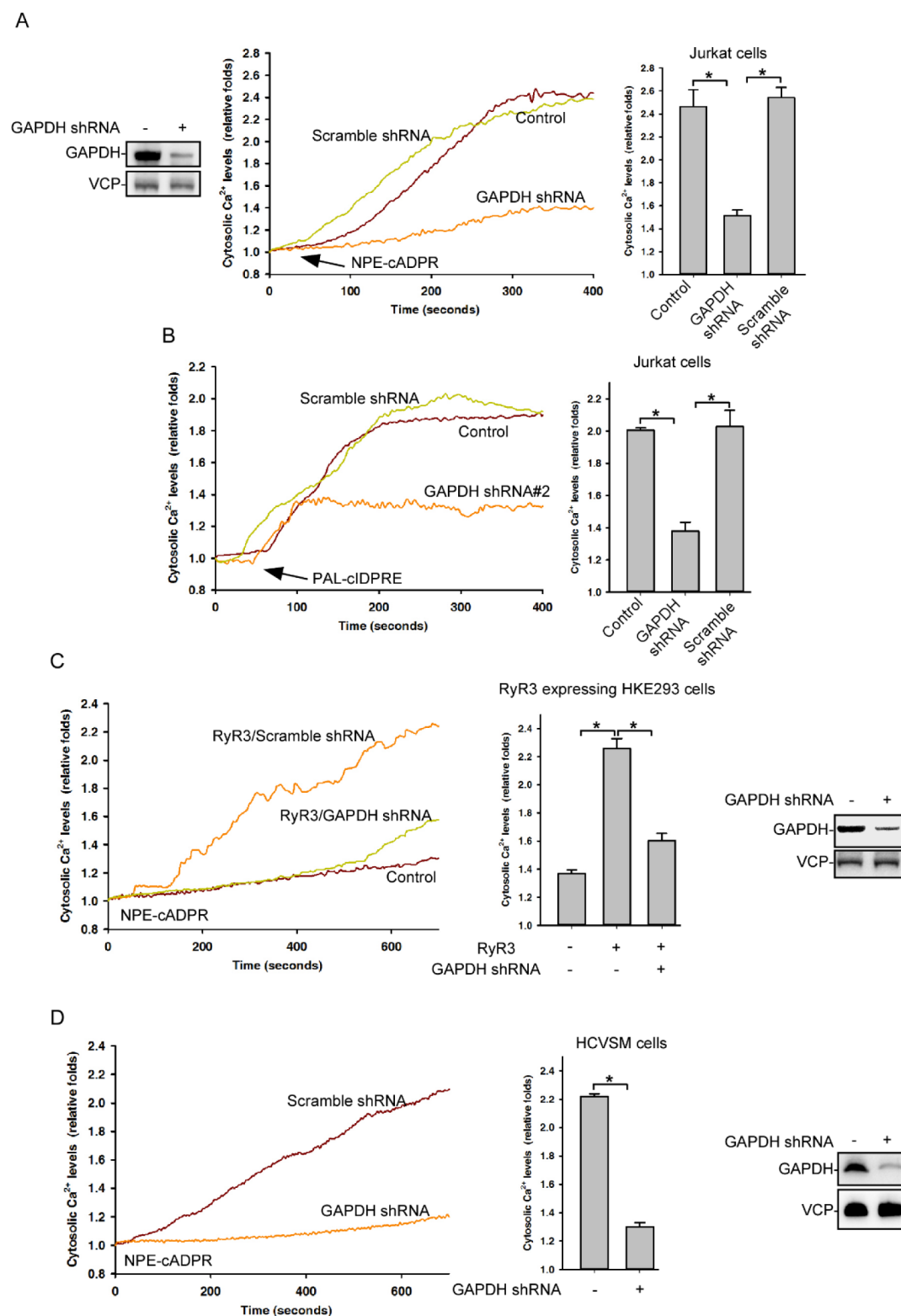


Figure 7. GAPDH is required for cADPR-induced Ca^{2+} mobilization in mammalian cells (A) and (B) GAPDH knockdown in Jurkat cells significantly inhibited NPE-cADPR ($200 \mu\text{M}$)-induced (A) or PAL-cIDPRE (1 mM)-induced (B) cytosolic Ca^{2+} increases. (C) and (D) GAPDH knockdown markedly inhibited NPE-cADPR ($200 \mu\text{M}$)-induced cytosolic Ca^{2+} increases in RyR3 expressing HEK293 cells (C) or HCVSM cells (D). Quantification of intracellular Ca^{2+} peak values are expressed as mean \pm S.D., $n = 3$ (15–30 cells in each independent experiment). *, $P < 0.05$.

RyRs form a class of intracellular calcium channels in various cells and tissues such as muscles and neurons. It is the major cellular mediator of calcium-induced calcium release in cells, a key event for triggering muscle contraction.³⁷ It is

thought that the final functional output of RyRs is determined by a complex interplay of fluctuating Ca^{2+} levels, tonic and short-lived cytosolic modulators, and protein–protein interactions. For example, FKBP12 binds to a closed state of RyRs

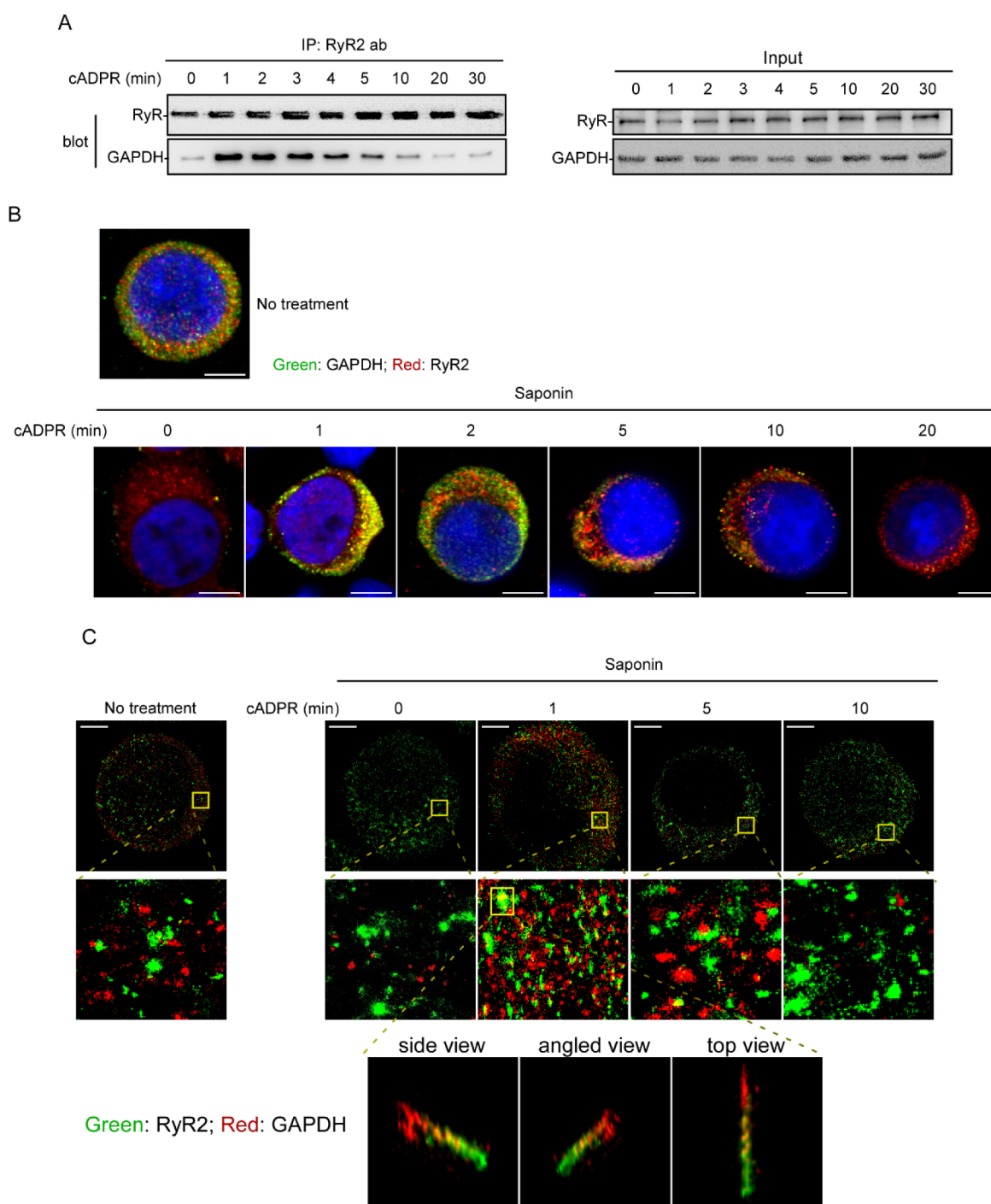


Figure 8. cADPR transiently increases the interaction between GAPDH and RyRs in human Jurkat cells. (A) cADPR (0.5 mM) transiently induced the increases of interaction between GAPDH and RyRs in Jurkat cell extract. (B) and (C) Treatment of saponin-permeabilized Jurkat cells with cADPR (0.5 mM) transiently induced the colocalization of GAPDH with RyR as shown by confocal image (B) or super-resolution image (C) analyses of GAPDH and RyR. Scale bar in (B) = 5 μm ; scale bar in (C) = 2.4 μm .

and thus decreases the sensitivity of RyRs to Ca^{2+} .³⁸ Along this line, the structure of a closed state RyR1 in complex with FKBP12 was recently determined by single-particle electron cryomicroscopy,³⁹ and this closed state RyR1 structure shed light on high ion conductance by RyRs and the long-range allosteric regulation of channel activities. It has been suggested that cADPR treatment induces the disassociation of FKBP12 from RyR2 and thus activates RyRs for Ca^{2+} releasing, and phosphorylation of RyR2 at Ser2808 or Ser2815 might be required for the release of FKBP12 from RyR2 as well.⁴⁰

Thus, it is of interest to assess the effects of the binding between cADPR and GAPDH on FKBP12's association with RyRs and the phosphorylation state of RyRs.

cADPR binding to GAPDH might induce a conformation change on GAPDH as revealed by the molecule docking and molecular dynamic simulations (Figure 4A), and obviously, this awaits to be confirmed by the crystal structure of GAPDH-cADPR complex. We also found that two regions in RyR2, residues 2210–2643 and residues 3512–4560, exhibited weak interaction with GAPDH *in vitro* (Figure

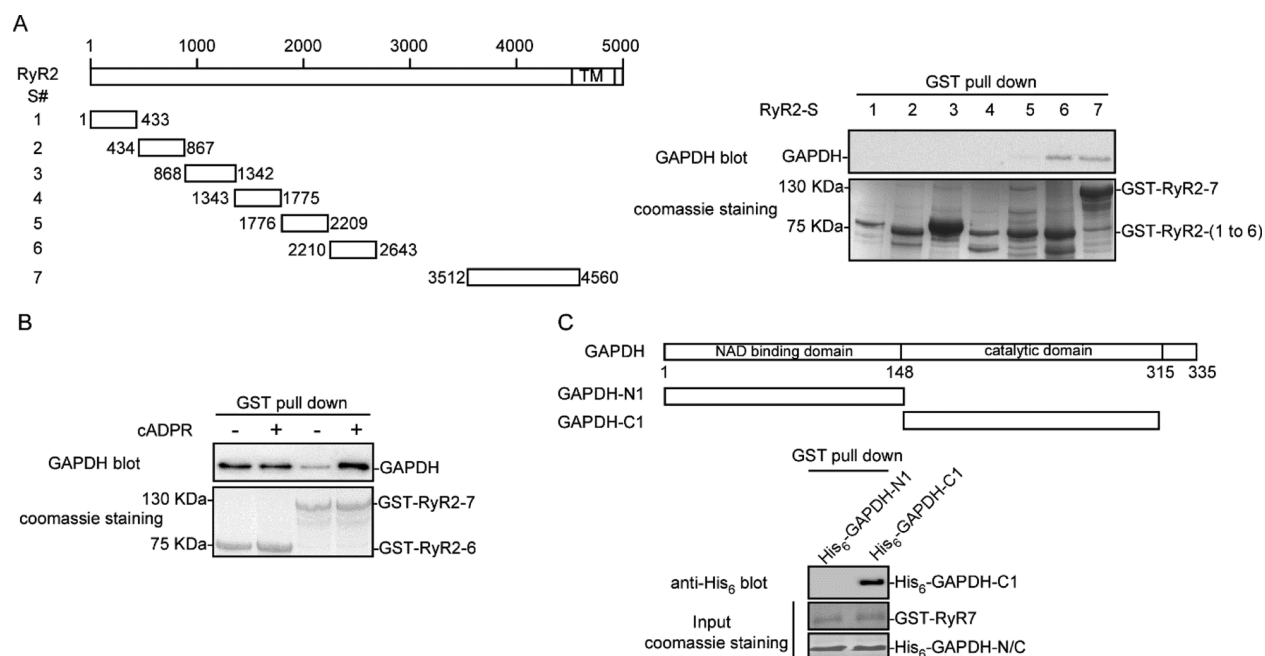


Figure 9. Mapping the regions in RyRs for GAPDH interaction *in vitro*. (A) GST pull-down assay on the *in vitro* interaction between GAPDH and various GST-RyR2 segments. (B) cADPR addition increased the interaction between RyR2-S7 and GAPDH *in vitro*. (C) GST pull-down assay on the *in vitro* interaction between GAPDH segments and the GST-RyR2-S7 segment.

9A). Surprisingly, cADPR addition only increased *in vitro* the binding affinity between region 7 of RyR2 and GAPDH, but not between region 6 of RyR2 and GAPDH (Figure 9B). One possibility is that the RyR2 region 6 fails to fold correctly *in vitro* resulting in the inability of the cADPR-GAPDH complex to efficiently interact with it. Another possibility is that cADPR binds to GAPDH and thus changes GAPDH's binding pattern with RyRs, showing higher affinity with one region in RyRs than another one. Additional *in vivo* assays are needed to assess these possibilities, and the ultimate answer might lie on solving the cryo-EM structure of cADPR–GAPDH–RyRs complex.

Glucose or glycolytic pathway intermediaries has long been found to modulate intracellular Ca²⁺ oscillation. For example, intracellular glucose inhibited cADPR-mediated Ca²⁺ spiking but potentiated IP₃-induced Ca²⁺ spiking.⁴¹ Several glycolytic enzymes, including GAPDH, have also been shown to form a ternary complex in skeletal muscle triads.⁴² Here we found that there is a weak interaction between GAPDH and RyRs in the absence cADPR (Figure S8A) and that cADPR treatment transiently increased the interaction between GAPDH and RyRs (Figures 8A,C and S8B). Not surprisingly, GAPDH knockdown markedly inhibited the ability of caffeine, a known RyRs agonist, to induce intracellular Ca²⁺ release in both Jurkat cells and RyR3-expressing HEK293 cells (Figure S9), suggesting that GAPDH is important for RyRs-mediated Ca²⁺ release in general.

Accumulating evidence indicates that GAPDH is more than just a catalyzing enzyme, functioning across the major cellular compartments to play essential roles in many important cellular events, such as DNA repair, tRNA export, membrane fusion and transport, cytoskeletal dynamics, and cell death.³² Indeed, dysregulation of GAPDH has been associated with numerous human diseases, e.g., neurodegenerative disorders and cancers.⁴³ It would be of interest to study whether the cADPR–GAPDH–RyR–Ca²⁺ cascade contributes to these

functions and disorders. The pleiotropic functions of GAPDH are regulated by post-translational modification and subcellular localization of GAPDH,⁴⁴ yet the mechanism underlying the regulation of GAPDH in these nonglycolytic cellular events remains elusive. The presumably conformational changes of GAPDH (Figure 4A) and its translocation to ER upon cADPR binding (Figures 8B,C) should add another layer of regulation on GAPDH.

■ ASSOCIATED CONTENT

📄 Supporting Information

The Supporting Information is available free of charge on the ACS Publications website at DOI: 10.1021/jacs.6b08088.

Primer sequences used in the study, synthesis scheme of azide-biotin and characterization of PAL-cIDPRE, purification of the cADPR binding proteins by a photoaffinity purification approach, purification and quantification of recombinant GAPDH wildtype, GAPDH^{His179Ala}, and GAPDH^{Arg234Ala} proteins, ADPR failed to specifically bind to GAPDH in the SPR assay, characterization of recombinant GAPDH wildtype, GAPDH^{His179Ala}, and GAPDH^{Arg234Ala} proteins by blue native (BN)-PAGE electrophoresis, effects of cADPR on the catalytic activity of GAPDH *in vitro*, cADPR transiently increases the interaction between GAPDH and RyRs in human Jurkat cells, GAPDH was required for caffeine (20 mM)-induced Ca²⁺ increases in mammalian cells (PDF)

■ AUTHOR INFORMATION

Corresponding Authors

*E-mail: zdszlh@bjmu.edu.cn.

*E-mail: liangren@bjmu.edu.cn.

*E-mail: jianbyue@cityu.edu.hk.

ORCID 

Jianbo Yue: 0000-0001-6384-5447

Funding

This work was supported by Hong Kong Research Grant Council (RGC) grants (785213 and 17126614), ITS/261/14, CAS-Croucher Funding Scheme, and Guangdong-Hong Kong joint innovation Research Scheme (#2016A050503010) to J.Y., research grants from Shenzhen government and from SUSTC (ZDSYS20140509142721429 and FRG-SUSTC1501A-24) to H.Z., and National Natural Science Foundation of China (NSFC) 91213302, 81673279 (to L.Z.) and 81573273 (to L-H.Z.).

Notes

The authors declare no competing financial interest.

ACKNOWLEDGMENTS

We thank members of Yue lab for their advice on the preparation of this manuscript.

REFERENCES

- (1) (a) Guse, A. H. *Curr. Med. Chem.* **2004**, *11*, 847–55. (b) Galione, A.; Churchill, G. C. *Sci. Signaling* **2000**, *2000*, PE1.
- (2) Bruzzone, S.; Moreschi, L.; Usai, C.; Guida, L.; Damonte, G.; Salis, A.; Scarfi, S.; Millo, E.; De Flora, A.; Zocchi, E. *Proc. Natl. Acad. Sci. U. S. A.* **2007**, *104*, 5759–64.
- (3) (a) Yilmaz, O. H.; Katajisto, P.; Lammung, D. W.; Gultekin, Y.; Bauer-Rowe, K. E.; Sengupta, S.; Birsoy, K.; Dursun, A.; Yilmaz, V. O.; Selig, M.; Nielsen, G. P.; Mino-Kenudson, M.; Zukerberg, L. R.; Bhan, A. K.; Deshpande, V.; Sabatini, D. M. *Nature* **2012**, *486*, 490–5. (b) Igarashi, M.; Guarente, L. *Cell* **2016**, *166*, 436–450.
- (4) Dodd, A. N.; Gardner, M. J.; Hotta, C. T.; Hubbard, K. E.; Dalchau, N.; Love, J.; Assie, J. M.; Robertson, F. C.; Jakobsen, M. K.; Goncalves, J.; Sanders, D.; Webb, A. A. *Science* **2007**, *318*, 1789–92.
- (5) Reyes-Harde, M.; Empson, R.; Potter, B. V.; Galione, A.; Stanton, P. K. *Proc. Natl. Acad. Sci. U. S. A.* **1999**, *96*, 4061–6.
- (6) (a) Yamasaki, M.; Thomas, J. M.; Churchill, G. C.; Garnham, C.; Lewis, A. M.; Cancela, J. M.; Patel, S.; Galione, A. *Curr. Biol.* **2005**, *15*, 874–8. (b) Kannan, M. S.; Fenton, A. M.; Prakash, Y. S.; Sieck, G. C. *Am. J. Physiol.* **1996**, *270*, H801–H806. (c) Prakash, Y. S.; Kannan, M. S.; Walseth, T. F.; Sieck, G. C. *Am. J. Physiol.* **1998**, *274*, C1653–C1660.
- (7) (a) Lee, H. C. *Curr. Mol. Med.* **2004**, *4*, 227–37. (b) Malavasi, F.; Deaglio, S.; Funaro, A.; Ferrero, E.; Horenstein, A. L.; Ortolan, E.; Vaisitti, T.; Aydin, S. *Physiol. Rev.* **2008**, *88*, 841–86. (c) Deterre, P.; Berthelot, V.; Bauvois, B.; Dalloul, A.; Schuber, F.; Lund, F. *Chem. Immunol.* **2000**, *75*, 146–68.
- (8) (a) Jin, D.; Liu, H. X.; Hirai, H.; Torashima, T.; Nagai, T.; Lopatina, O.; Shnyder, N. A.; Yamada, K.; Noda, M.; Seike, T.; Fujita, K.; Takasawa, S.; Yokoyama, S.; Koizumi, K.; Shiraishi, Y.; Tanaka, S.; Hashii, M.; Yoshihara, T.; Higashida, K.; Islam, M. S.; Yamada, N.; Hayashi, K.; Noguchi, N.; Kato, I.; Okamoto, H.; Matsushima, A.; Salmina, A.; Munesue, T.; Shimizu, N.; Mochida, S.; Asano, M.; Higashida, H. *Nature* **2007**, *446*, 41–5. (b) Nagamune, K.; Hicks, L. M.; Fux, B.; Brossier, F.; Chini, E. N.; Sibley, L. D. *Nature* **2008**, *451*, 207–10.
- (9) Koch-Nolte, F.; Haag, F.; Guse, A. H.; Lund, F.; Ziegler, M. *Sci. Signaling* **2009**, *2*, mr1.
- (10) (a) Galione, A.; Lee, H. C.; Busa, W. B. *Science* **1991**, *253*, 1143–6. (b) Galione, A.; White, A.; Willmott, N.; Turner, M.; Potter, B. V.; Watson, S. P. *Nature* **1993**, *365*, 456–9. (c) Hua, S. Y.; Tokimasa, T.; Takasawa, S.; Furuya, Y.; Nohmi, M.; Okamoto, H.; Kuba, K. *Neuron* **1994**, *12*, 1073–9. (d) Barry, V. A.; Cheek, T. R. *Biochem. J.* **1994**, *300*, 589–97. (e) Lee, H. C.; Aarhus, R.; Graeff, R. M. *J. Biol. Chem.* **1995**, *270*, 9060–9066. (f) Noguchi, N.; Takasawa, S.; Nata, K.; Tohgo, A.; Kato, I.; Ikehata, F.; Yonekura, H.; Okamoto, H. *J. Biol. Chem.* **1997**, *272*, 3133–6. (g) Kunerth, S.; Langhorst, M. F.; Schwarzmann, N.; Gu, X.; Huang, L.; Yang, Z.; Zhang, L.; Mills, S. J.; Zhang, L. H.; Potter, B. V.; Guse, A. H. *J. Cell Sci.* **2004**, *117*, 2141–2149. (h) Fulceri, R.; Rossi, R.; Bottinelli, R.; Conti, A.; Intravaia, E.; Galione, A.; Benedetti, A.; Sorrentino, V.; Reggiani, C. *Biochem. Biophys. Res. Commun.* **2001**, *288*, 697–702.
- (11) Thomas, J. M.; Masgrau, R.; Churchill, G. C.; Galione, A. *Biochem. J.* **2001**, *359*, 451–457.
- (12) (a) Walseth, T. F.; Aarhus, R.; Kerr, J. A.; Lee, H. C. *J. Biol. Chem.* **1993**, *268*, 26686–26691. (b) Tang, W. X.; Chen, Y. F.; Zou, A. P.; Campbell, W. B.; Li, P. L. *Am. J. Physiol. Heart Circ. Physiol.* **2002**, *282*, H1304–10.
- (13) Gu, X.; Yang, Z.; Zhang, L.; Kunerth, S.; Fliegert, R.; Weber, K.; Guse, A. H.; Zhang, L. *J. Med. Chem.* **2004**, *47*, 5674–82.
- (14) Wei, W.; Lu, Y.; Hao, B.; Zhang, K.; Wang, Q.; Miller, A. L.; Zhang, L. R.; Zhang, L. H.; Yue, J. *Stem Cells* **2015**, *33*, 2664–73.
- (15) Lu, Y.; Hao, B. X.; Graeff, R.; Wong, C. W.; Wu, W. T.; Yue, J. *J. Biol. Chem.* **2013**, *288*, 24247–63.
- (16) Lu, Y.; Dong, S.; Hao, B.; Li, C.; Zhu, K.; Guo, W.; Wang, Q.; Cheung, K. H.; Wong, C. W.; Wu, W. T.; Markus, H.; Yue, J. *Autophagy* **2014**, *10*, 1895–905.
- (17) Zhao, T.; Wang, Y.; Zhai, Y.; Qu, X.; Cheng, A.; Du, S.; Loy, M. M. *Opt. Express* **2015**, *23*, 1879–87.
- (18) Yue, J.; Ferrell, J. E., Jr. *Mol. Cell. Biol.* **2006**, *26*, 5300–9.
- (19) Sybyl X 1.1.2 *Molecular Modeling Suite*, version 1.1.2; BioPharmic, LLC: San Mateo, CA, 2009.
- (20) *GOLD docking program*, version 5.2.2; CCDC Software Ltd.: Cambridge, U.K., 2013.
- (21) Zhang, J.; Snyder, S. H. *Proc. Natl. Acad. Sci. U. S. A.* **1992**, *89*, 9382–5.
- (22) Graeff, R.; Liu, Q.; Kriksunov, I. A.; Kotaka, M.; Oppenheimer, N.; Hao, Q.; Lee, H. C. *J. Biol. Chem.* **2009**, *284*, 27629–36.
- (23) Sambrook, J.; Russell, D. W. *Cold Spring Harb. Protoc.* **2006**, *2006*, 3757.
- (24) Niepmann, M.; Zheng, J. *Electrophoresis* **2006**, *27*, 3949–51.
- (25) (a) Tsuzuki, T.; Sakaguchi, N.; Kudoh, T.; Takano, S.; Uehara, M.; Murayama, T.; Sakurai, T.; Hashii, M.; Higashida, H.; Weber, K.; Guse, A. H.; Kameda, T.; Hirokawa, T.; Kumaki, Y.; Potter, B. V.; Fukuda, H.; Arisawa, M.; Shuto, S. *Angew. Chem., Int. Ed.* **2013**, *52*, 6633–7. (b) Swarbrick, J. M.; Graeff, R.; Garnham, C.; Thomas, M. P.; Galione, A.; Potter, B. V. *Chem. Commun.* **2014**, *50*, 2458–61.
- (26) Zhang, L.; Yue, J.; Zhang, L. H. *Chem. Rec.* **2015**, *15*, 511–23.
- (27) (a) Higashida, H.; Salmina, A. B.; Olovyanikova, R. Y.; Hashii, M.; Yokoyama, S.; Koizumi, K.; Jin, D.; Liu, H. X.; Lopatina, O.; Amina, S.; Islam, M. S.; Huang, J. J.; Noda, M. *Neurochem. Int.* **2007**, *51*, 192–9. (b) Lee, H. C.; Aarhus, R.; Graeff, R.; Gurnack, M. E.; Walseth, T. F. *Nature* **1994**, *370*, 307–9.
- (28) Yu, P. L.; Zhang, Z. H.; Hao, B. X.; Zhao, Y. J.; Zhang, L. H.; Lee, H. C.; Zhang, L.; Yue, J. *J. Biol. Chem.* **2012**, *287*, 24774–83.
- (29) (a) Cowan-Jacob, S. W.; Kaufmann, M.; Anselmo, A. N.; Stark, W.; Grutter, M. G. *Acta Crystallogr., Sect. D: Biol. Crystallogr.* **2003**, *59*, 2218–27. (b) Charron, C.; Talfournier, F.; Isupov, M. N.; Littlechild, J. A.; Branlant, G.; Vitoux, B.; Aubry, A. *J. Mol. Biol.* **2000**, *297*, 481–500.
- (30) Lee, H. C.; Aarhus, R.; Levitt, D. *Nat. Struct. Biol.* **1994**, *1*, 143–4.
- (31) Seidler, N. W. *Adv. Exp. Med. Biol.* **2013**, *985*, 1–36.
- (32) (a) Chang, C.; Su, H.; Zhang, D.; Wang, Y.; Shen, Q.; Liu, B.; Huang, R.; Zhou, T.; Peng, C.; Wong, C. C.; Shen, H. M.; Lippincott-Schwartz, J.; Liu, W. *Mol. Cell* **2015**, *60*, 930–40. (b) Yun, J.; Mullarky, E.; Lu, C.; Bosch, K. N.; Kavalier, A.; Rivera, K.; Roper, J.; Chio, I.; Giannopoulou, E. G.; Rago, C.; Muley, A.; Asara, J. M.; Paik, J.; Elemento, O.; Chen, Z.; Pappin, D. J.; Dow, L. E.; Papadopoulos, N.; Gross, S. S.; Cantley, L. C. *Science* **2015**, *350*, 1391–6.
- (33) (a) des Georges, A.; Clarke, O. B.; Zalk, R.; Yuan, Q.; Condon, K. J.; Grassucci, R. A.; Hendrickson, W. A.; Marks, A. R.; Frank, J. *Cell* **2016**, *167*, 145–157. (b) Peng, W.; Shen, H.; Wu, J.

Guo, W.; Pan, X.; Wang, R.; Chen, S. R.; Yan, N. *Science* **2016**, *354*, aah5324.

- (34) Lee, H. C. *J. Biol. Chem.* **1991**, *266*, 2276–2281.
- (35) Guse, A. H.; da Silva, C. P.; Berg, I.; Skapenko, A. L.; Weber, K.; Heyer, P.; Hohenegger, M.; Ashamu, G. A.; Schulze-Koops, H.; Potter, B. V.; Mayr, G. W. *Nature* **1999**, *398*, 70–3.
- (36) Pattnaik, P. *Appl. Biochem. Biotechnol.* **2005**, *126*, 79–92.
- (37) (a) Franzini-Armstrong, C.; Protasi, F. *Physiol. Rev.* **1997**, *77*, 699–729. (b) Protasi, F.; Shtifman, A.; Julian, F. J.; Allen, P. D. *Am. J. Physiol. Cell Physiol.* **2004**, *286*, 662C–670C. (c) Yano, M.; Yamamoto, T.; Ikeda, Y.; Matsuzaki, M. *Nat. Clin. Pract. Cardiovasc. Med.* **2006**, *3*, 43–52.
- (38) Marx, S. O.; Reiken, S.; Hisamatsu, Y.; Jayaraman, T.; Burkhoff, D.; Rosemblyt, N.; Marks, A. R. *Cell* **2000**, *101*, 365–76.
- (39) (a) Zalk, R.; Clarke, O. B.; des Georges, A.; Grassucci, R. A.; Reiken, S.; Mancina, F.; Hendrickson, W. A.; Frank, J.; Marks, A. R. *Nature* **2014**, *517*, 44–49. (b) Efremov, R. G.; Leitner, A.; Aebersold, R.; Raunser, S. *Nature* **2014**, *517*, 39–43. (c) Yan, Z.; Bai, X. C.; Yan, C.; Wu, J.; Li, Z.; Xie, T.; Peng, W.; Yin, C. C.; Li, X.; Scheres, S. H.; Shi, Y.; Yan, N. *Nature* **2014**, *517*, 50–55.
- (40) (a) Zheng, J.; Wenzhi, B.; Miao, L.; Hao, Y.; Zhang, X.; Yin, W.; Pan, J.; Yuan, Z.; Song, B.; Ji, G. *Cell Calcium* **2010**, *47*, 449–57. (b) Zhang, X.; Tallini, Y. N.; Chen, Z.; Gan, L.; Wei, B.; Doran, R.; Miao, L.; Xin, H. B.; Kotlikoff, M. I.; Ji, G. *Cardiovasc. Res.* **2009**, *84*, 253–62. (c) Wang, Y.-X.; Zheng, Y.-M.; Mei, Q.-B.; Wang, Q.-S.; Collier, M. L.; Fleischer, S.; Xin, H.-B.; Kotlikoff, M. I. *Am. J. Physiol.: Cell Physiol.* **2004**, *286*, C538–C546.
- (41) (a) Chini, E. N.; Dousa, T. P. *Arch. Biochem. Biophys.* **1999**, *370*, 294–9. (b) Cancela, J. M.; Mogami, H.; Tepikin, A. V.; Petersen, O. H. *Curr. Biol.* **1998**, *8*, 865–8.
- (42) Brandt, N. R.; Caswell, A. H.; Wen, S. R.; Talvenheimo, J. A. *J. Membr. Biol.* **1990**, *113*, 237–51.
- (43) (a) Suzuki, M.; Sasabe, J.; Miyoshi, Y.; Kuwasako, K.; Muto, Y.; Hamase, K.; Matsuoka, M.; Imanishi, N.; Aiso, S. *Proc. Natl. Acad. Sci. U. S. A.* **2015**, *112*, E2217–24. (b) Sen, N.; Hara, M. R.; Kornberg, M. D.; Cascio, M. B.; Bae, B. I.; Shahani, N.; Thomas, B.; Dawson, T. M.; Dawson, V. L.; Snyder, S. H.; Sawa, A. *Nat. Cell Biol.* **2008**, *10*, 866–73.
- (44) (a) Sawa, A.; Khan, A. A.; Hester, L. D.; Snyder, S. H. *Proc. Natl. Acad. Sci. U. S. A.* **1997**, *94*, 11669–74. (b) Tristan, C.; Shahani, N.; Sedlak, T. W.; Sawa, A. *Cell. Signalling* **2011**, *23*, 317–23. (c) Hara, M. R.; Agrawal, N.; Kim, S. F.; Cascio, M. B.; Fujimuro, M.; Ozeki, Y.; Takahashi, M.; Cheah, J. H.; Tankou, S. K.; Hester, L. D.; Ferris, C. D.; Hayward, S. D.; Snyder, S. H.; Sawa, A. *Nat. Cell Biol.* **2005**, *7*, 665–74.